AGU PUBLICATIONS

Geophysical Research Letters

RESEARCH LETTER
10.1002/2016GL068050

Key Points:
- A slab avalanche event occurred beneath Southeast Asia during the early Miocene
- The slab avalanche event induced observed large-scale synchronous basin inversion and subsidence
- Mantle dynamics may play important role in regional basin evolution

Supporting Information:
- Tables S1–S3 and Figures S1–S6

Correspondence to:
T. Yang,
tyang@gps.caltech.edu

Citation:
Yang, T., M. Gurnis, and S. Zahirovic (2016), Mantle-induced subsidence and compression in SE Asia since the early Miocene, *Geophys. Res. Lett., 43*, 1901–1909, doi:10.1002/2016GL068050.

Received 31 JAN 2016
Accepted 15 FEB 2016
Accepted article online 17 FEB 2016
Published online 5 MAR 2016

Mantle-induced subsidence and compression in SE Asia since the early Miocene

Ting Yang[1], Michael Gurnis[1], and Sabin Zahirovic[2]

[1]Seismological Laboratory, California Institute of Technology, Pasadena, California, USA, [2]EarthByte Group, School of Geosciences, University of Sydney, Sydney, New South Wales, Australia

Abstract Rift basins developed extensively across Sundaland, the continental core of Southeast Asia, since the Eocene. Beginning in the early Miocene, basins in southern Sundaland experienced widespread synchronous compression (inversion) and marine inundation, despite a large drop in long-term global sea level. The mechanism for this large-scale synchronous regional sea level rise, basin inversion, and subsidence is not well understood and contrary to expectations from traditional basin models and eustatic sea level trends. We present geodynamic models of mantle convection with both deformable and rigid plate reconstructions to investigate this enigma. Models suggest that a slab stagnates within the transition zone beneath Southeast Asia before the Miocene. The stagnant slab penetrated through the 660 km mantle discontinuity during the early Miocene and formed a slab avalanche event, due to continuous subduction and accumulation of negatively buoyant slabs. This avalanche may have induced large-scale marine inundation, regional compression, and basin inversion across southern Sundaland. We argue mantle convection induced large-scale basin compression, in contrast to conventional plate margin-induced compression; this suggests mantle convection may exert a much stronger control on surface processes than previously recognized.

1. Introduction

Southeast Asia's continental core, Sundaland (Figure 1a), is an amalgamation of tectonic blocks which assembled since the Late Paleozoic [*Metcalfe*, 2013; *Zahirovic et al*., 2014]. Although seismicity and present internal deformation is small [*Simons et al*., 2007], high surface heat flux, low seismic velocity within the lithosphere and uppermost mantle suggests that Sundaland has experienced widespread deformation in the past [*Hall and Morley*, 2004]. Sundaland is characterized by widely distributed basin extension since the late Eocene [*Hall and Morley*, 2004; *Doust and Sumner*, 2007] (Figure 1b) and basin inversion since the early Miocene [*Hall and Morley*, 2004; *Doust and Sumner*, 2007] (Figure 1c). During basin inversion, formerly extensional basins are compressed and shortened and thus are usually accompanied by uplift and erosion [*Ziegler*, 1987; *Lowell*, 1995]. The basin inversion was most intense within the southern parts of Sundaland (Figure 1c). For example, there was only minor inversion in Gulf of Thailand, while further south in the Malay and West Natuna basins, inversion was more significant [*Hall and Morley*, 2004; *Doust and Sumner*, 2007] (Figure 1c). Although basin inversion is often accompanied by uplift and erosion [*Ziegler*, 1987; *Lowell*, 1995], the Sunda shelf became entirely marine, and the sedimentary facies changed from terrestrial to shallow marine during this inversion [*Hall and Morley*, 2004; *Doust and Sumner*, 2007] (Figures 1b and 1c), despite long-term falling eustatic sea level [*Haq and Al-Qahtani*, 2005; *Spasojevic and Gurnis*, 2012]. The coincidence of this large-scale basin inversion, marine inundation in the context of a long-term global sea level fall, is puzzling and suggests controls beyond plate tectonics and traditional concepts invoking stretching and compression of the crust and lithosphere.

Seismic tomography shows a voluminous near-horizontal high-velocity anomaly within the lower mantle beneath Southeast Asia [*Li et al*., 2008; *Simmons et al*., 2012] (Figures 1d, 1e, and S1 in the supporting information). The high-velocity anomaly, ~2500 km long (EW direction) and ~1500 wide (NS direction) at ~ 1200 km depth (the middle depth of the generally horizontal anomaly, Figure S1), coincides in location with the large-scale synchronous basin inversion and subsidence across southern Sundaland (Figure 1c). The horizontal slab remains connected to the subducting Indo-Australian Plate [*Li et al*., 2008; *Simmons et al*., 2012] (Figures 1d and 1e). This slab morphology and depth distribution is reminiscent to that following so-called mantle avalanche events from computational models [*Zhong and Gurnis*, 1995; *Pysklywec and Mitrovica*, 1998; *Pysklywec and Ishii*, 2005]. In the slab avalanche, the subducted slab is initially inhibited from penetrating through the 660 km phase change from the spinel structure to perovskite [*Zhong and Gurnis*, 1995;

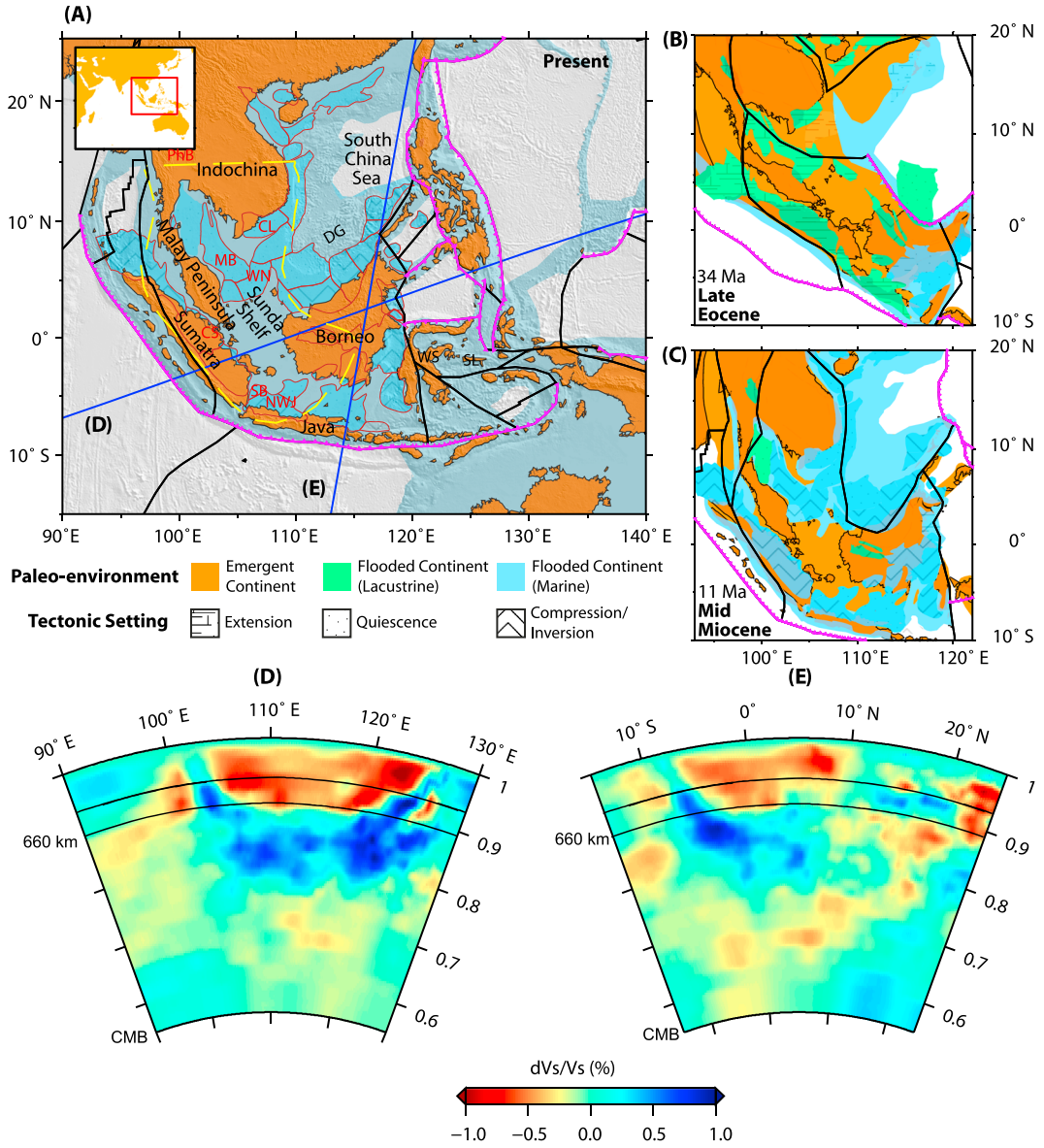

Figure 1. Paleogeography [*Golonka et al.*, 2006] and basin evolution [*Doust and Sumner*, 2007] in Southeast Asia at (a) present, (b) late Eocene, and middle Miocene (c). Southeast Asian Tertiary basins [*Doust and Sumner*, 2007] are outlined by red lines. Evolutions of the average dynamic topography and lithosphere stress within the yellow dashed line are demonstrated in Figure 4. Convergent and divergent and transform boundaries are represented by pink and black lines, respectively. Oceanic plates are represented as white in (b and c). (d and e) Cross section of *P* wave [*Li et al.*, 2008] seismic velocity anomalies. Red letters in Figure 1a mark abbreviations for sedimentary basins: CL, Cuu Long; CS, central Sumatra; MB, Malay; NWJ, Northwest Java; PhB, Phitsanulok; SB: Sunda; WN, West Natuna. Black letters mark tectonic blocks. Abbreviations are the following: DG, Dangerous Ground; SL: Sula; SW: Sulawesi.

Christensen, 1996] and lies subhorizontally within the transition zone. The stagnating slab accumulates mass by continuous subduction until its negative buoyancy exceeds the support of the phase boundary. The previously impeded slab begins to penetrate into the lower mantle while inducing a strong downwelling flow, which drags down the topography and compresses the overriding lithosphere [*Zhong and Gurnis*, 1995; *Pysklywec and Mitrovica*, 1998; *Pysklywec and Ishii*, 2005].

Usually, plate tectonics, lithospheric deformation, and related isostatic responses dominate the observed total topography. For example, assuming that the lithosphere is in isostatic equilibrium, the computed surface topography is usually a good approximation to the observed topography. However, lithospheric

deformation alone cannot explain the large-scale synchronous basin inversion and marine inundation across southern Sundaland. Mantle flow and related dynamic topography (surface undulation induced by mantle convection) might have significantly affected the paleogeography of Southeast Asia, as demonstrated by the very low dynamic topography at present from numerical models [e.g., *Flament et al*. [2013]] and recently compiled residual topography [*Winterbourne et al*., 2014]. We investigate the dynamics of Sundaland since the Eocene (50 Ma) with a four-dimensional (3-D plus time) geodynamic model with assimilation of plate reconstruction information [*Flament et al*., 2014; *Bower et al*., 2015] while accounting for basin stretching, plate tectonics, and mantle convection. Sundaland's extensive and complex deformation since the Cenozoic is incorporated (Figure S2) within a global rigid plate reconstruction [*Zahirovic et al*., 2014]. The global rigid plate reconstruction uses continuously closing plates in which each plate polygon changes shape through the motion of individual plate boundaries [*Gurnis et al*., 2012]. This combination of rigid and deforming plates enables us to study details of lithospheric-scale deformation induced topography evolution under the background of large-scale mantle convection.

2. Methods

2.1. Mantle Convection Model

Dynamical evolution of the mantle system is governed by partial differential equations for conservation of mass, momentum and energy and advection of composition [*McNamara and Zhong*, 2004]. Solving the fully dynamic, self-consistent mantle convection problem is computationally expensive, so we resort to several simplifications. We assume the mantle is incompressible and satisfies the Boussinesq approximation and solve mantle evolution with the finite element method using CitcomS [*Zhong et al*., 2000], modified to progressively assimilate surface horizontal velocities, lithospheric thermal structure, and subducting slab thermal structure in the shallow mantle based on tectonic reconstructions [*Bower et al*., 2015]. Compared to models using time-dependent surface horizontal velocity boundary conditions only, e.g., *Bunge et al*. [1998], this hybrid technique ensures that the buoyancy flux is consistent with the plate reconstructions [*Bower et al*., 2015]. Although the mantle convection model is not fully self-consistent, the predicted quantities (e.g., present day mantle structure, dynamic topography, and topography evolution) are consistent with geological and geophysical data [*Flament et al*., 2014; *Shephard et al*., 2014]. To minimize the influence of side boundaries on mantle flow, the model domain size is set as $120° \times 120° \times 2890$ km, spanning from 55° to 175°E and 60°S to 60°N, with Sundaland lying in the middle of the model domain. We use a mesh of $128 \times 128 \times 64$ with horizontal refinement in Southeast Asia (~50 km resolution between 90° to 130°E and 10°S to 20°N) and vertical refinement in the top and bottom boundary layers (~10 km resolution in the shallowest layer). Physical constants used in this study are listed in Table S1.

Continental lithosphere and crust have different chemical compositions from the surrounding mantle. Because the surface topography and crustal thickness are not well constrained in the past and we mainly focus on the relative change of topography, the initial continental crustal at 50 Ma is set to a homogeneous layer with a thickness of 40 km (the average present continental crust thickness [*Christensen and Mooney*, 1995]). The continental lithosphere is divided into three types based on the tectonothermal ages: Archean, Proterozoic and Phanerozoic. The chemical lithosphere thickness and density deficiency of these four regions are 250 km, 160 km and 130 km and 1%, 0.7% and 0.5%, respectively [*Artemieva and Mooney*, 2001; *Kaban et al*., 2003; *Artemieva*, 2009]. The corresponding thermal lithosphere is defined from the half space-cooling model with thermal age of 360 Ma, 150 Ma, and 100 Ma, respectively. This choice of the lithospheric thermal age makes the initial surface total topography nearly flat [*Flament et al*., 2014].

Mantle viscosity and initial mantle temperature have significant influence on mantle evolution. We derive the initial mantle temperature at 50 Ma (Figure S3b) by integrating backward [*Spasojevic and Gurnis*, 2012] an estimate of the present temperature structure (Figure S3a), which is synthesized from S40RTS tomography model [*Ritsema et al*., 2011] and slab model RUM [*Gudmundsson and Sambridge*, 1998]. The present mantle temperature structure together with the temperature- and depth-dependent viscosity structure is inverted by optimizing the fit of the geoid, free-air gravity, gradient of gravity in three orthogonal directions and residual topography in ocean basins (Table S2). Although the geoid, free-air gravity, gradients of gravity are all derived from the gravitational field, they are sensitive to structures with different depths and scales. Because the mantle structure inversion is not unique, we checked for the effects of different inverted mantle

viscosity and mantle temperature structure and tomography models. The related model parameters are listed in Table S2.

Using the estimate of the mantle state at 50 Ma (Figure S3), we integrate forward in time with a 4-D plate tectonic assimilation technique [*Flament et al*., 2014; *Bower et al*., 2015] to investigate evolution of the slab, surface topography, and horizontal stress within the lithosphere. At each time step, slab thermal structure above 350 km depth is determined from plate reconstructions [*Bower et al*., 2015]. Below a depth of 350 km or away from the slab, mantle thermal structure evolves dynamically [*Bower et al*., 2015].

To calculate mantle flow-induced dynamic topography and lithospheric horizontal stress at specific ages, we (1) eliminate the buoyancy and lateral viscosity variations above 250 km depth, (2) change the top mechanical boundary condition from prescribed velocity to free-slip boundary condition, and then restart the model to calculate the instantaneous mantle flow and related quantities (surface dynamic topography and lithospheric horizontal stress) assuming that the surface is water loaded [*Flament et al*., 2013]. We acknowledge that eliminating heterogeneity in the top 250 km is a simplification, but large-scale dynamic topography is mainly affected by mantle structure beneath the isostatically compensated shallow layer [*Hager and Richards*, 1989]. One example is the long-wavelength geoid, which does not resemble surface topography and mainly reflects density heterogeneity within the mantle and its induced dynamic topography. Besides, lithospheric heterogeneity (crustal thickness, lithosphere temperature, and lithosphere thickness variations) induced by tectonic evolution (Figure S2) is used to construct isostatic topography [*McKenzie*, 1977], which is combined with dynamic topography to predict the basin subsidence history (Figure S4). The averaged horizontal viscous stress (average of the maximum and minimum horizontal principal stress at 10 km depth) can serve as an indication of the lithosphere tectonic mechanism [*Steinberger et al*., 2001]. The lithosphere is under tension (compression) if the average horizontal stress is positive (negative).

2.2. Deforming Plate Model and Basin Subsidence

Sundaland experienced a complex lithospheric deformation history during the Cenozoic. We construct a deforming network for Sundaland (Figure S2), which is embedded into a global rigid plate reconstruction model [*Zahirovic et al*., 2014]. Although including a deforming plate model does not have a significant influence on the large-scale mantle structure evolution, it enables us to study basin subsidence history within the background of large-scale mantle convection. The motion within the deforming network is controlled by plate boundaries and a number of control features [*Flament et al*., 2014], including rigid blocks and basin boundaries (Figure S2). The relative motion between rigid blocks, which experienced little internal deformation during the Cenozoic is inherited from previous reconstructions [*Lee and Lawver*, 1994; *Hall*, 2002; *Seton et al*., 2012; *Zahirovic et al*., 2014] which compile paleomagnetic, structural, and gravity data for reconstruction. The relative motion between basin boundaries is inferred based on the basin tectonic subsidence curves [*Pigott and Sattayarak*, 1993; *Madon and Watts*, 1998; *Doust and Sumner*, 2007]. Basin subsidence is dominated by lithospheric extension and subsequent long-term cooling [*McKenzie*, 1978]. However, dynamic topography also affects basin subsidence [*Lithgow-Bertelloni and Gurnis*, 1997]. To remove the effect of dynamic topography from observed tectonic subsidence, we first calculate mantle flow and corresponding dynamic topography evolution with the rigid plate reconstruction as the top boundary. Then we subtract dynamic topography from the observed basin subsidence curve for each basin and derive lithospheric deformation- and cooling-related basin subsidence. We invert for strain rate, basin extension, and basin boundaries relative motion history for each basin by fitting the observed basin tectonic subsidence curves [*Cochran*, 1983; *White*, 1994]. The inverted basin tectonic history is listed in Table S3. Figure S2 demonstrates our reconstructed deforming plate at 30 Ma and the present.

3. Results

Before the Miocene, a horizontal slab stagnates above the 660 km boundary beneath Southeast Asia (Figure 2a, 30 Ma). Subducted slabs from circum-Sunda subduction zones (e.g., Sunda Trench and the trench at northern Borneo, Figure 2) progressively add negative buoyancy to the stagnant slab (Figure S5). During the early Miocene, the accumulated slab within the transition zone begins to penetrate through the 660 km boundary and enters the lower mantle, forming a slab avalanche (Figures 2b and 2c). The slab avalanche is evident in the velocity field (Figure 2) and the slab-sinking rates beneath Sundaland (Figure 3), which demonstrate significant increase since the early Miocene (e.g., the slab-sinking rate beneath Sundaland increased from ~1.1 cm/yr at 20 Ma to ~2.2 cm/yr at 0 Ma). From 50 Ma to the present, the modeled cold slab sinks to

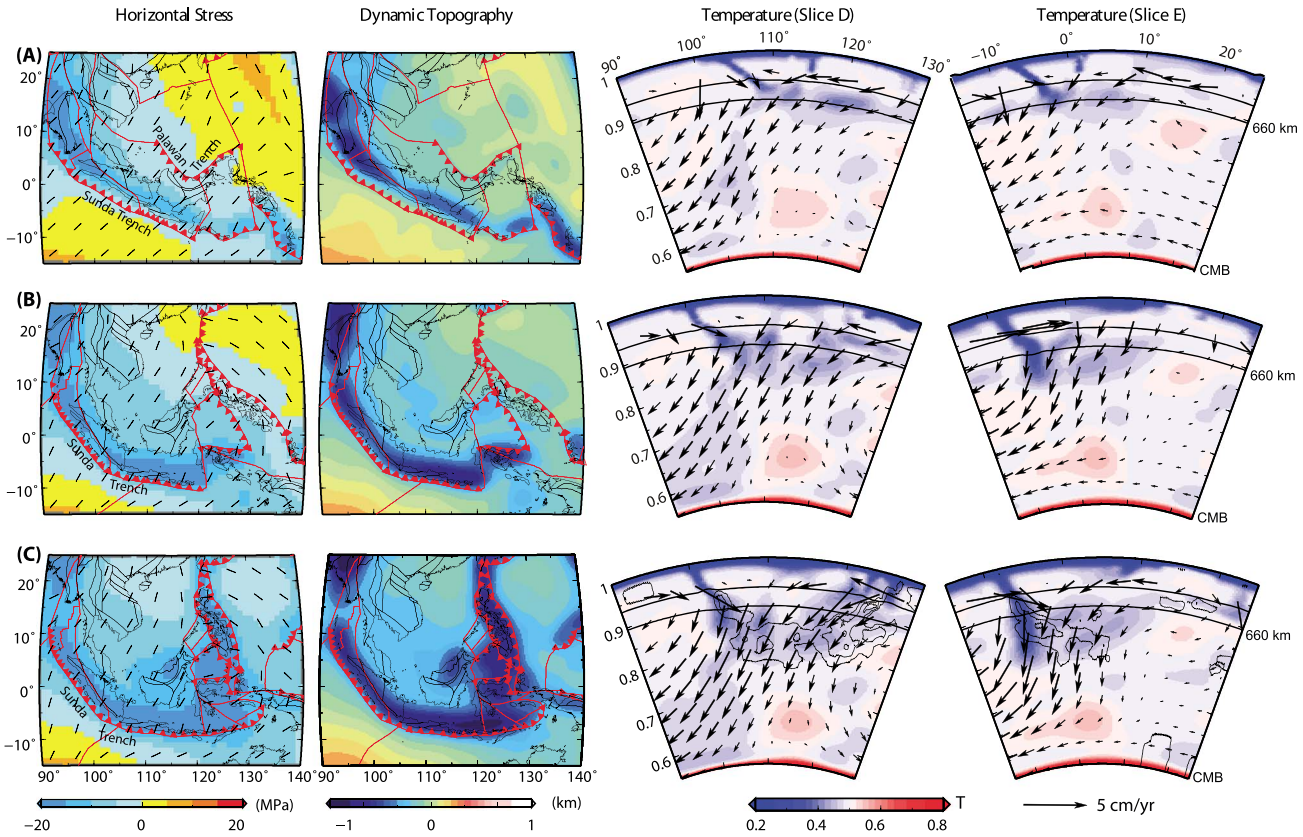

Figure 2. (first column) Lithospheric horizontal stress field, (second column) dynamic topography, and (third and fourth columns) temperature at (a) 30 Ma, (b) 10 Ma, and (c) 0 Ma for Case 1 (see Table S2). Negative and positive stress amplitudes represent horizontal compression and extension respectively. Black bar represents the maximum principal stress direction. The temperature slices are fixed to the mantle frame, and their locations are labeled in Figure 1a. Black contour lines in temperature cross sections at 0 Ma represent +0.3% *P* wave [*Li et al.*, 2008] velocity perturbation.

~1200 km depth (Figure 2c). Although the background large-scale temperature structure is synthesized from seismic models, most of the predicted present slab material is generated by the continuous subduction surrounding Sundaland (Figure S5). The predicted present slab morphology beneath Southeast Asia is consistent with the high-resolution *P* wave tomography [*Li et al.*, 2008] (Figure 2c). Accompanying the modeled slab avalanche since the early Miocene, southern Sundaland experiences broadscale compression and dynamic subsidence (Figure 2), induced by the strong downwelling viscous flow [*Zhong and Gurnis*, 1995; *Pysklywec and Mitrovica*, 1998; *Pysklywec and Ishii*, 2005].

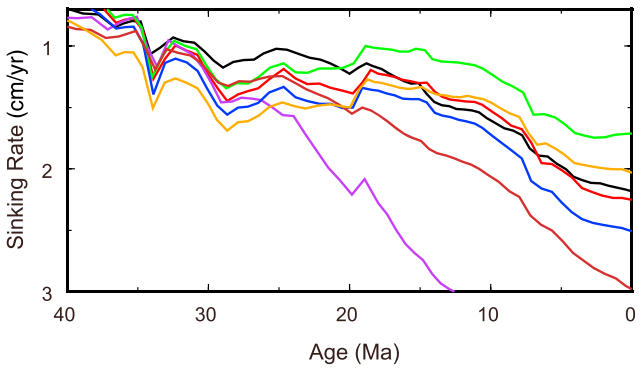

Figure 3. The slab sinking rate between 620 and 700 km depth and beneath Sundaland averaged at each age. Black, red, violet, green, blue, brown, and orange colors represent results from Cases 1 to 7, respectively (Table S2).

Consistent with the long-term eustatic sea level fall, the fraction of continental crust experiencing marine inundation globally decreases progressively since the Eocene [*Heine et al.*, 2015] (Figure 4a). However, flooding within Sundaland increases since the Eocene (Figure 4a), in contrast to the eustatic sea level and global emergence of continental crust. Our calculations show that the average dynamic topography in Sundaland continued to decrease since the Eocene (Figures 2 and 4b), consistent with the trend of Sundaland's abnormal flooding history. The amplitude of this subsidence

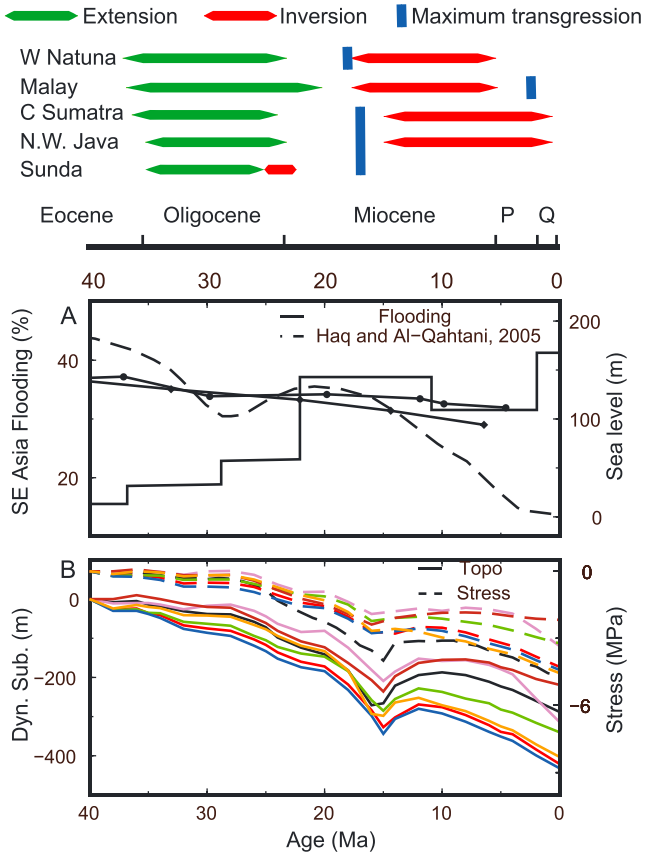

Figure 4. (a) Sundaland flooding area percent and eustatic sea level [*Haq and Al-Qahtani*, 2005] since the Eocene. Sundaland flooding area percent is calculated based on paleogeographic maps [*Golonka et al.*, 2006] with method similar as *Heine et al.* [2015]. As a comparison, global continental crust flooding area percent [*Heine et al.*, 2015] is also plotted (solid diamond or circles). (b) Sundaland average dynamic subsidence (solid line) and stress evolution (dashed line). Yellow dashed line in Figure 1a outlines the present extent of the averaging region, the shape, and location of which evolves with time. Black, red, violet, green, blue, brown, and orange colors represent results from Cases 1 to 7, respectively (Table S2). Above Figure 4a, extension, inversion and maximum marine transgression history for several basins within southern Sundaland [*Doust and Sumner*, 2007] are shown. The time scale for the stratigraphic ages is also provided. P and Q represent Pliocene and Quaternary, respectively.

is a few hundred meters, exceeding the eustatic sea level decrease (Figure 4a) and would contribute to a transition from subaerial erosion to marine sedimentation in southern Sundaland since the early Miocene (Figures 1b and 1c), as reconstructed in paleogeographic maps and geological syntheses [*Hall and Morley*, 2004; *Doust and Sumner*, 2007]. The broadscale compression (Figures 2 and 4b) helps to explain the extensive basin inversion across southern Sundaland since the early Miocene. The subsidence of the dynamic topography and compression of the horizontal stress amplitude accelerate since the late Oligocene to early Miocene in Sundaland (Figure 4b), consistent with the transition from extension to inversion and a peak in marine transgression in southern Sundaland [*Hall and Morley*, 2004; *Doust and Sumner*, 2007] (Figure 4).

We examine the basin subsidence history and mantle convection-induced horizontal stress amplitude at six wells across Sundaland (Figure S4). Although lithospheric processes dominate the basin subsidence history, dynamic topography in southern Sundaland (e.g., Sunda and Central Sumatra basins) has a significant influence on modeled basin subsidence within. For example, besides lithosphere extension-induced subsidence, the decreasing of dynamic topography has induced ~400 m more tectonic subsidence in the Sunda basin. In contrast, in northern Sundaland (e.g., Phitsanulok and Cuu Long basins), modeled dynamic topography has a smaller influence on basin subsidence history.

Lithospheric horizontal principal stress is controlled by a combination of plate boundary, topographic, and mantle convection related forces. Mantle flow-induced lithospheric horizontal principal stress directions are perpendicular to the trench near the subduction zones, consistent with observed regional principal stress direction (Figure S6). Inside Sundaland, the inconsistency between the predicted and observed principal stress directions increases from south (near the trench) to north (far from the trench) (Figure S6), suggesting gradually increased effects of other forces (e.g., plate boundary and topographic forces). The latitudinal trend in dynamic topography and horizontal stress amplitude within the basins (Figure S4), horizontal stress direction (Figure S6) and history of basin inversion [*Doust and Sumner*, 2007] (Figure 1c) suggests that subducted slabs, which lie beneath southern Sundaland (Figures 1e and S1), mainly affect dynamic topography, lithospheric stress, basin (rifting or inversion) regime, and subsidence in southern Sundaland.

Mantle convection is affected by several poorly constrained physical parameters, and the mantle structure inversion is not unique. We determined the influences of different reference viscosities, Clapeyron slopes at the 660 km phase boundary, viscosity and temperature structures, and tomographic inversions on our results.

The reference viscosity controls the mantle flow velocity while the Clapeyron slope affects the stagnation of the slab. Our preferred reference viscosity (2.5×10^{22} Pa s) is close to previously inferred average lower mantle viscosity (~3×10^{22} to 4×10^{22} Pa s) [*Forte et al.*, 1991; *Čížková et al.*, 2012]. Reducing the reference viscosity from our preferred value of 2.5×10^{22} to 1.0×10^{22} Pa s significantly shifts the avalanche time from ~20 Ma to ~35 Ma while inducing more vigorous downwelling flow (Figure 3). On the other hand, increasing the reference viscosity to 5.0×10^{22} Pa s yields milder downwelling flow (Figure 3). The estimated Clapeyron slope at the 660 km boundary mainly varies between −1 and −3 K/MPa [*Tauzin and Ricard*, 2014]. Considering the nonunique characteristics of inverted mantle properties, we investigate the dynamical evolution of Sundaland with different viscosity profiles or temperature to seismic velocity ratios. Reducing the Clapeyron slope from our preferred −2.5 K/MPa to −1.5 K/MPa, using a different temperature structure (through a different tomography models to construct the present day temperature structure or using different temperature-seismic velocity ratios, Table S2) or using different viscosity structure (Table S2), does not affect our inference that there was an early horizontal-lying slab within the transition zone which subsequently penetrated into the lower mantle while inducing large-scale synchronous subsidence and compression across southern Sundaland (Figure 3).

4. Discussion and Conclusion

Although basin inversion plays an important role in tectonics, basin thermal histories, and petroleum generation and preservation within sedimentary basins, its mechanism is still not fully understood. The horizontal, in-plate compressive stress fields responsible for basin inversion are normally explained by plate-scale forces related to plate tectonics and plate boundary forces [*Ziegler*, 1987; *Lowell*, 1995]. For example, collision at the northern (between the Dangerous Ground and north Borneo, Figure 1) and eastern (between Sulawesi and Sula, Figure 1) Indonesia and interplate coupling has been invoked to explain the basin inversion [*Letouzey et al.*, 1990] and uplift [*Molnar and Cronin*, 2015] in eastern Sunda shelf since the middle Miocene. However, plate-boundary forces cannot explain the synchronous marine inundation in southern Sundaland since the early Miocene. In contrast, downwelling mantle flow can explain the synchronous regional basin inversion and sea level rise across southern Sundaland.

Mantle flow-induced dynamic topography (vertical stress) has previously been used to explain long-wavelength vertical motion and flooding of continental interiors [*Lithgow-Bertelloni and Gurnis*, 1997; *Zhang et al.*, 2012], and mantle flow-induced lithospheric horizontal stress field has also been invoked to explain extensional [*Lithgow-Bertelloni and Guynn*, 2004] or compressional tectonics [*Lithgow-Bertelloni and Guynn*, 2004; *Pik et al.*, 2008; *Yamato et al.*, 2013]. However, the influence of mantle downwelling on large-scale basin evolution has seldom been noted. We show that a slab avalanche-induced downwelling flow accounts for the synchronous large-scale compression, basin inversion, and subsidence in southern Sundaland. Thus, mantle flow not only affects the large-scale vertical motion and flooding history but also plays an important role in the large-scale lithospheric stress state and tectonic regime [*Lithgow-Bertelloni and Guynn*, 2004; *Yamato et al.*, 2013]. Tomography images a present-day snapshot of mantle convection and reveals that subducted slabs are often impeded at the 660 km discontinuity [*Li et al.*, 2008; *Simmons et al.*, 2012] and arguably stagnate within the transition zone. Periodic slab avalanches, occurring at different locations, as suggested by tomography [*Li et al.*, 2008; *Simmons et al.*, 2012] and numerical models [*Zhong and Gurnis*, 1995], would likely periodically induce major changes in mantle flow, topography, continental tectonic regimes, and stratigraphy. However, a slab avalanche is a transient process and the long-term geological signature is likely to be an unconformity rather than a thick sedimentary sequence [*Burgess and Gurnis*, 1995].

In conclusion, we suggest that a stagnant slab, which lay horizontally in the transition zone beneath Southeast Asia before the Miocene, became unstable and penetrated into the lower mantle in the early Miocene, forming a slab avalanche event. The strong downwelling flow generated by the slab avalanche induced the concurrent marine inundation and inversion across southern Sundaland.

Acknowledgments
We thank S. Williams and R.D. Müller for their discussions and Laurent Husson and Grace Shephard for their helpful reviews. T.Y. and M.G. were supported by Statoil ASA and the NSF (through EAR-1247022 and EAR-1028978), and S.Z. was supported by ARC grant IH130200012. Readers can contact the corresponding author to request all the data used in this paper.

References

Artemieva, I. M. (2009), The continental lithosphere: Reconciling thermal, seismic, and petrologic data, *Lithos*, *109*(1), 23–46.
Artemieva, I. M., and W. D. Mooney (2001), Thermal thickness and evolution of Precambrian lithosphere: A global study, *J. Geophys. Res.*, *106*(B8), 16,387–16,414.

Bower, D. J., M. Gurnis, and N. Flament (2015), Assimilating lithosphere and slab history in 4-D Earth models, *Phys. Earth Planet. Inter.*, *238*, 8–22.
Bunge, H.-P., M. A. Richards, C. Lithgow-Bertelloni, J. R. Baumgardner, S. P. Grand, and B. A. Romanowicz (1998), Time scales and heterogeneous structure in geodynamic Earth models, *Science*, *280*(5360), 91–95.
Burgess, P. M., and M. Gurnis (1995), Mechanisms for the formation of cratonic stratigraphic sequences, *Earth Planet. Sci. Lett.*, *136*(3), 647–663.
Christensen, N., and W. Mooney (1995), Seismic velocity structure and composition of the continental crust: A global view, *J. Geophys. Res.*, *100*(B7), 9761–9788.
Christensen, U. R. (1996), The influence of trench migration on slab penetration into the lower mantle, *Earth Planet. Sci. Lett.*, *140*(1), 27–39.
Čížková, H., A. P. van den Berg, W. Spakman, and C. Matyska (2012), The viscosity of Earth's lower mantle inferred from sinking speed of subducted lithosphere, *Phys. Earth Planet. Inter.*, *200*, 56–62.
Cochran, J. R. (1983), Effects of finite rifting times on the development of sedimentary basins, *Earth Planet. Sci. Lett.*, *66*, 289–302.
Doust, H., and H. S. Sumner (2007), Petroleum systems in rift basins—A collective approach in Southeast Asian basins, *Petrol. Geosci.*, *13*(2), 127–144.
Flament, N., M. Gurnis, and R. D. Müller (2013), A review of observations and models of dynamic topography, *Lithosphere*, *5*(2), 189–210.
Flament, N., M. Gurnis, S. Williams, M. Seton, J. Skogseid, C. Heine, and R. D. Müller (2014), Topographic asymmetry of the South Atlantic from global models of mantle flow and lithospheric stretching, *Earth Planet. Sci. Lett.*, *387*, 107–119.
Forte, A., W. Peltier, and A. Dziewonski (1991), Inferences of mantle viscosity from tectonic plate velocities, *Geophys. Res. Lett.*, *18*(9), 1747–1750.
Golonka, J., M. Krobicki, J. Pająk, N. Van Giang, and W. Zuchiewicz (2006), *Global Plate Tectonics and Paleogeography of Southeast Asia*, AGH University of Science and Technology, Arkadia, Krakow, Poland.
Gudmundsson, Ó., and M. Sambridge (1998), A regionalized upper mantle (RUM) seismic model, *J. Geophys. Res.*, *103*(B4), 7121–7136.
Gurnis, M., M. Turner, S. Zahirovic, L. DiCaprio, S. Spasojevic, R. D. Müller, J. Boyden, M. Seton, V. C. Manea, and D. J. Bower (2012), Plate tectonic reconstructions with continuously closing plates, *Comput. Geosci.*, *38*(1), 35–42.
Hager, B., and M. Richards (1989), Long-wavelength variations in Earth's geoid: Physical models and dynamical implications, *Philos. Trans. R. Soc. London, Ser. A*, *328*(1599), 309–327.
Hall, R. (2002), Cenozoic geological and plate tectonic evolution of SE Asia and the SW Pacific: Computer-based reconstructions, model and animations, *J. Asian Earth Sci.*, *20*(4), 353–431.
Hall, R., and C. K. Morley (2004), Sundaland basins, in *Continent-Ocean Interactions within East Asian Marginal Seas*, *Geophys. Monogr. Ser.*, edited by P. Clift et al., pp. 55–85, AGU, Washington, D. C.
Haq, B. U., and A. M. Al-Qahtani (2005), Phanerozoic cycles of sea-level change on the Arabian Platform, *Geoarabia*, *10*(2), 127–160.
Heine, C., L. Yeo, and R. Müller (2015), Evaluating global paleoshoreline models for the Cretaceous and Cenozoic, *Aust. J. Earth Sci.*, *62*, 275–287, doi:10.1080/08120099.08122015.01018321.
Kaban, M. K., P. Schwintzer, I. M. Artemieva, and W. D. Mooney (2003), Density of the continental roots: Compositional and thermal contributions, *Earth Planet. Sci. Lett.*, *209*(1), 53–69.
Lee, T.-Y., and L. A. Lawver (1994), Cenozoic plate reconstruction of the South China Sea region, *Tectonophysics*, *235*(1), 149–180.
Letouzey, J., P. Werner, and A. Marty (1990), Fault reactivation and structural inversion. Backarc and intraplate compressive deformations. Example of the eastern Sunda shelf (Indonesia), *Tectonophysics*, *183*(1), 341–362.
Li, C., R. D. van der Hilst, E. R. Engdahl, and S. Burdick (2008), A new global model for *P* wave speed variations in Earth's mantle, *Geochem. Geophys. Geosyst.*, *9*, Q05018, doi:10.1029/2007GC001806.
Lithgow-Bertelloni, C., and M. Gurnis (1997), Cenozoic subsidence and uplift of continents from time-varying dynamic topography, *Geology*, *25*(8), 735–738.
Lithgow-Bertelloni, C., and J. H. Guynn (2004), Origin of the lithospheric stress field, *J. Geophys. Res.*, *109*, B01408, doi:10.1029/2003JB002467.
Lowell, J. D. (1995), Mechanics of basin inversion from worldwide examples, in *Basin Inversion*, edited by J. G. Buchanan and P. G. Buchanan, *Geol. Soc. London, Spec. Publ.*, pp. 39–57.
Madon, M. B., and A. Watts (1998), Gravity anomalies, subsidence history and the tectonic evolution of the Malay and Penyu Basins (offshore Peninsular Malaysia), *Basin Res.*, *10*(4), 375–392.
McKenzie, D. (1977), Surface deformation, gravity anomalies and convection, *Geophys. J. Int.*, *48*(2), 211–238.
McKenzie, D. (1978), Some remarks on the development of sedimentary basins, *Earth Planet. Sci. Lett.*, *40*(1), 25–32.
McNamara, A. K., and S. Zhong (2004), Thermochemical structures within a spherical mantle: superplumes or piles? *J. Geophys. Res.*, *109*, B07402, doi:10.1029/2003JB002847.
Metcalfe, I. (2013), Gondwana dispersion and Asian accretion: Tectonic and palaeogeographic evolution of eastern Tethys, *J. Asian Earth Sci.*, *66*, 1–33.
Molnar, P., and T. W. Cronin (2015), Growth of the Maritime Continent and its possible contribution to recurring Ice Ages, *Paleoceanography*, *30*, 196–225, doi:10.1002/2014PA002752.
Pigott, J. D., and N. Sattayarak (1993), Aspects of sedimentary basin evolution assessed through tectonic subsidence analysis. Example: Northern Gulf of Thailand, *J. Southeast Asian Earth Sci.*, *8*(1), 407–420.
Pik, R., B. Marty, J. Carignan, G. Yirgu, and T. Ayalew (2008), Timing of East African Rift development in southern Ethiopia: Implication for mantle plume activity and evolution of topography, *Geology*, *36*(2), 167–170.
Pysklywec, R. N., and J. X. Mitrovica (1998), Mantle flow mechanisms for the large-scale subsidence of continental interiors, *Geology*, *26*(8), 687–690.
Pysklywec, R. N., and M. Ishii (2005), Time dependent subduction dynamics driven by the instability of stagnant slabs in the transition zone, *Phys. Earth Planet. Inter.*, *149*(1), 115–132.
Ritsema, J., A. Deuss, H. Van Heijst, and J. Woodhouse (2011), S40RTS: A degree-40 shear-velocity model for the mantle from new Rayleigh wave dispersion, teleseismic traveltime and normal-mode splitting function measurements, *Geophys. J. Int.*, *184*(3), 1223–1236.
Seton, M., R. Müller, S. Zahirovic, C. Gaina, T. Torsvik, G. Shephard, A. Talsma, M. Gurnis, M. Turner, and S. Maus (2012), Global continental and ocean basin reconstructions since 200Ma, *Earth Sci. Rev.*, *113*(3), 212–270.
Shephard, G., N. Flament, S. Williams, M. Seton, M. Gurnis, and R. Müller (2014), Circum-Arctic mantle structure and long-wavelength topography since the Jurassic, *J. Geophys. Res. Solid Earth*, *119*, 7889–7908.
Simmons, N. A., S. C. Myers, G. Johannesson, and E. Matzel (2012), LLNL-G3Dv3: Global *P* wave tomography model for improved regional and teleseismic travel time prediction, *J. Geophys. Res.*, *117*, B10302, doi:10.1029/2012JB009525.
Simons, W., A. Socquet, C. Vigny, B. Ambrosius, S. Haji Abu, C. Promthong, C. Subarya, D. Sarsito, S. Matheussen, and P. Morgan (2007), A decade of GPS in Southeast Asia: Resolving Sundaland motion and boundaries, *J. Geophys. Res.*, *112*, B06420, doi:10.1029/2005JB003868.

Spasojevic, S., and M. Gurnis (2012), Sea level and vertical motion of continents from dynamic earth models since the Late Cretaceous, *AAPG Bull.*, *96*(11), 2037–2064.
Steinberger, B., H. Schmeling, and G. Marquart (2001), Large-scale lithospheric stress field and topography induced by global mantle circulation, *Earth Planet. Sci. Lett.*, *186*(1), 75–91.
Tauzin, B., and Y. Ricard (2014), Seismically deduced thermodynamics phase diagrams for the mantle transition zone, *Earth Planet. Sci. Lett.*, *401*, 337–346.
White, N. (1994), An inverse method for determining lithospheric strain rate variation on geological timescales, *Earth Planet. Sci. Lett.*, *122*(3), 351–371.
Winterbourne, J., N. White, and A. Crosby (2014), Accurate measurements of residual topography from the oceanic realm, *Tectonics*, *33*, 982–1015, doi:10.1002/2013TC003372.
Yamato, P., L. Husson, T. W. Becker, and K. Pedoja (2013), Passive margins getting squeezed in the mantle convection vice, *Tectonics*, *32*, 1559–1570, doi:10.1002/2013TC003375.
Zahirovic, S., M. Seton, and R. Müller (2014), The Cretaceous and Cenozoic tectonic evolution of Southeast Asia, *Solid Earth*, *5*, 227–273.
Zhang, N., S. Zhong, and R. M. Flowers (2012), Predicting and testing continental vertical motion histories since the Paleozoic, *Earth Planet. Sci. Lett.*, *317*, 426–435.
Zhong, S., and M. Gurnis (1995), Mantle convection with plates and mobile, faulted plate margins, *Science*, *267*(5199), 838–843.
Zhong, S., M. T. Zuber, L. Moresi, and M. Gurnis (2000), Role of temperature-dependent viscosity and surface plates in spherical shell models of mantle convection, *J. Geophys. Res.*, *105*(B5), 11,063–11,082.
Ziegler, P. (1987), Late Cretaceous and Cenozoic intra-plate compressional deformations in the Alpine foreland—A geodynamic model, *Tectonophysics*, *137*(1), 389–420.